



Chemical compositions of impact melt breccias and target rocks from the Tenoumer impact crater, Mauritania

Giovanni PRATESI^{1,2*}, Marco MORELLI^{1,2}, Angelo Pio ROSSI³, and Gian Gabriele ORI³

¹Dipartimento di Scienze della Terra, Università degli Studi di Firenze, Via G. La Pira 4, 50121 Firenze, Italy

²Museo di Scienze Planetarie della Provincia di Prato, Via Galcianese, 59100 Prato, Italy

³International Research School of Planetary Sciences, Università d'Annunzio, Viale Pindaro 42, 65127 Pescara, Italy

*Corresponding author. E-mail: g.pratesi@unifi.it

(Received 10 May 2005; revision accepted 05 August 2005)

Abstract—The impact melt breccias from the Tenoumer crater (consisting of a fine-grained intergrowth of plagioclase laths, pyroxene crystals, oxides, and glass) display a wide range of porosity and contain a large amount of target rock clasts.

Analyses of major elements in impact melt rocks show lower contents of SiO₂, Al₂O₃, and Na₂O, and higher contents of MgO, Fe₂O₃, and CaO, than the felsic rocks (i.e., granites and gneisses) of the basement. In comparison with the bulk analyses of the impact melt, the glass is strongly enriched in Si-Al, whereas it is depleted both in Mg and Fe; moreover, the impact melt rocks are variably enriched or depleted in some REE with respect to the felsic and mafic bedrock types. Gold is slightly enriched in the impact melt, and Co, Cr, and Ni abundances are possibly due to a contribution from mafic bedrock.

Evidences of silicate-carbonate liquid immiscibility, mainly as spherules and globules of calcite within the silicate glass, have been highlighted.

HMX mixing calculation confirm that the impact melt rocks are derived from a mixing of at least six different target lithologies outcropping in the area of the crater. A large contribution is derived from granitoids (50%) and mica schist (17–19%), although amphibolites (~15%), cherty limestones (~10%), and ultrabasites (~6%) components are also present.

The very low abundances of PGE in the melt rock seem to come mainly from some ultrabasic target rocks; therefore, the contamination from the meteoritic projectile appears to have been negligible.

INTRODUCTION

The Tenoumer crater is a 1.9-km-wide impact structure located in Mauritania, in a remote area of the western Sahara Desert (22°55'N, 10°24'W). It represents one of only 20 currently known African impact structures (Koeberl 1994; Master and Reimold 2000; Paillou et al. 2004). Tenoumer appears as a circular depression bordered by a well-preserved rim rising about 100 m over the crater floor (Figs. 1 and 2). The crater is filled with unconsolidated sediments with a thickness of 200–300 m, according to geophysical measurements (Fudali and Cassidy 1972; Grieve et al. 1989). The inner slopes are very steep and locally abrupt; the outer slopes are steep and abrupt only in the upper part, whereas they flatten out, gently sloping into the surrounding plain, in the lower part.

The origin of the crater was long debated. Early studies of Tenoumer (Richard-Molard 1948) described the presence of basalt lava and pumice in a peripheral depression and favored an origin by volcanic explosion. The first suggestion of a possible origin by meteorite impact was made by Allix (1951), even though he was not able to provide confirming evidence for this hypothesis. On the basis of the occurrence of small dikes, which were supposed to be rhyodacitic lava, Monod and Pomerol (1966) suggested a possible volcanic origin for the structure. Finally, definitive evidence for the impact origin of this crater was supplied by French et al. (1970), who found up to eight sets of planar deformation features (PDFs) in quartz grains in inclusions of granitic basement scattered throughout the above-mentioned “lava.” Following this discovery the nature of this “lava” was re-evaluated by the same authors and interpreted as rapidly



Fig. 1. Panoramic view of the Tenoumer crater.

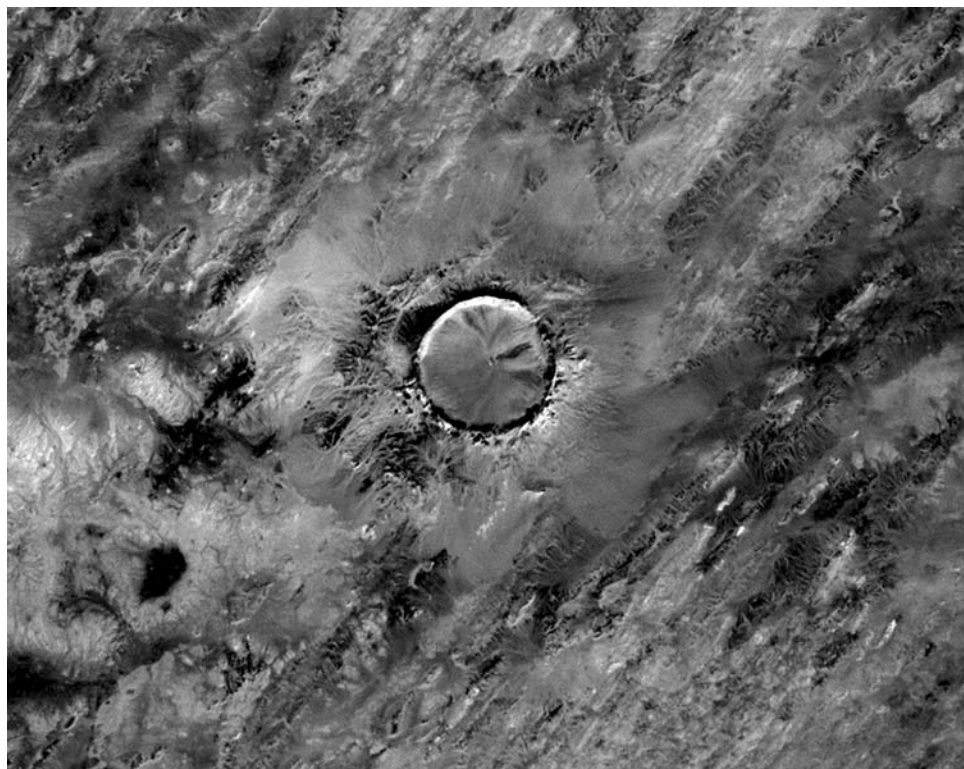


Fig. 2. Landsat image of the Tenoumer crater, Mauritania (after NASA, <https://zulu.ssc.nasa.gov/mrsid/mrsid.pl>).

quenched impact melt rock. French et al. (1970) carried out a detailed study of the mineralogy of these melt rocks and were able to establish the age of the Tenoumer crater as 2.5 ± 0.5 Ma by K/Ar dating of impact melt rock. This age has recently been revisited by Storzer et al. (2003), who pointed out the possible presence of inherited radiogenic Ar in the samples previously analyzed by French et al. (1970). Employing fission track analysis of apatite in impact melt rocks, they obtained an age of only 21.4 ± 9.7 ka. This result precludes the possibility that the Tenoumer and Aouelloul craters (Aouelloul is a 0.36-km-wide impact crater located in the Adrar region, Mauritania, and formed 3.1 ± 0.3 Ma ago; for more details see Koeberl et al. 1998) are genetically related and part of a multiple impact event, as was previously speculated by Dietz et al. (1969) and Fudali and Cressy (1976).

As concerns the overall geochemical characteristics of the Tenoumer melt rock, French et al. (1970) demonstrated with Rb-Sr isotopic data that the melt rocks are related to the basement rocks. A further contribution to the knowledge of this structure was made by Fudali (1974), who showed that the chemical composition of the impact melt rock was not identical to the composition of the gneissic and granitic basement rocks, probably due to contamination by an amphibolitic component found in the same area. However, no chemical analyses of minor and trace elements have been reported to date for either impact melt rock or target rock types.

During an expedition to Mauritania in November-December 2002, samples of impactite and basement rock were collected at Tenoumer crater. We have carried out a detailed geochemical study of these lithologies. Major and

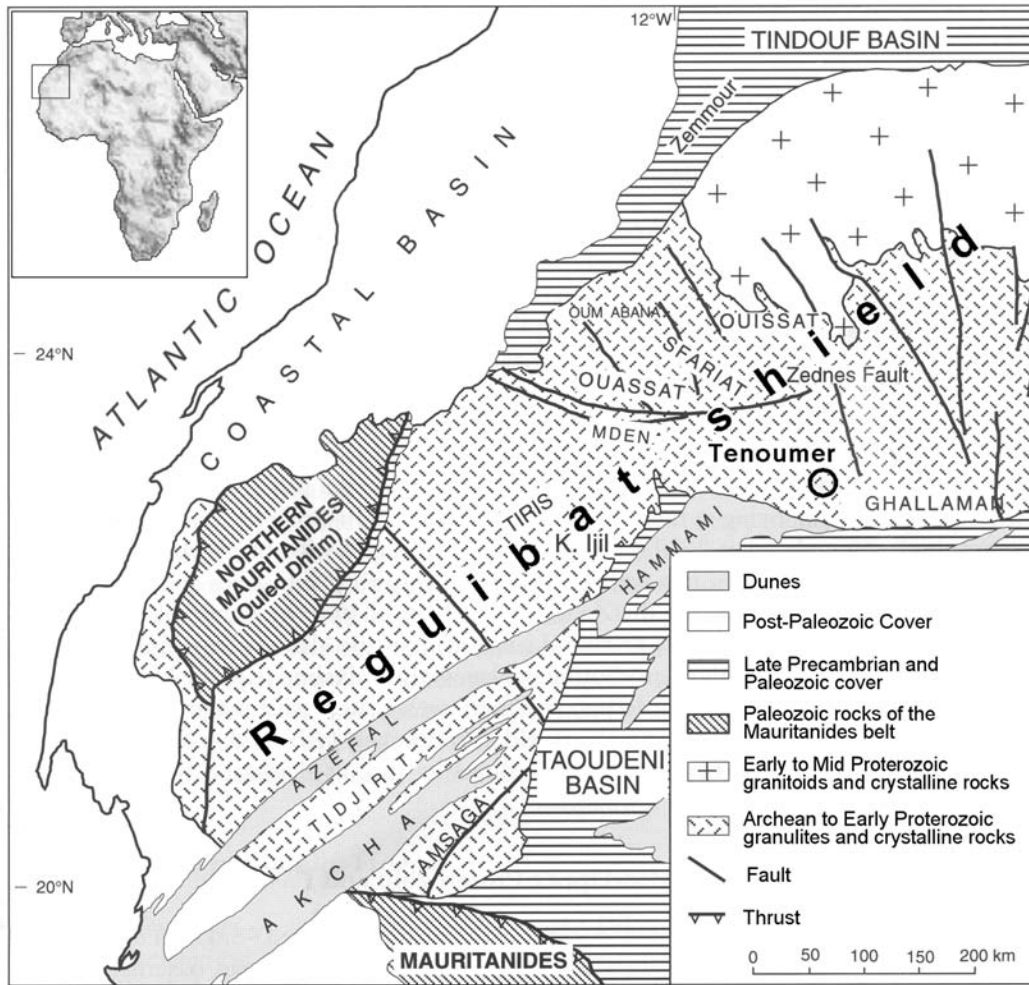


Fig. 3. Geological sketch map of the western Africa and Tenoumer crater location.

trace elements, including rare earth elements (REE) and platinum group elements (PGE), were measured in order to investigate a possible presence of a meteoritic signature in the melt, as well as to investigate the mixing of different components of country rocks.

GEOLOGICAL SETTING

Tenoumer crater is located on a peneplain extending for hundreds of kilometers along the southern margin of the Reguibat Shield (Fig. 3), a 1500 km long and 200–400 km wide zone where the basement of the Precambrian West African craton is exposed (Kennedy 1964). In this region, which has been quite stable for at least 1.7 Ga, the landscape is characterized by very rare inselberg and alternating erg and reg (sand or gravel dominated, respectively) desert. Adrar plateau escarpments, made up of Precambrian and Paleozoic successions, bound the Reguibat Shield to the south. The central and western portions of the Reguibat Shield consist of Archean and mid-Proterozoic migmatites, gneiss, rare

quartzites, and other siliceous and calcareous sedimentary units (Rocci et al. 1991; Piqué 2001). Amphibolites and gabbros are only locally present, whereas granitoids and pegmatite intrusions represent the most recent rocks of the crystalline basement. The age of metamorphism (Rocci et al. 1991) decreases from the west (about 3.3 Ga for granulite-facies metamorphism) to the east (about 2 Ga for green schists metamorphism); moreover, magmatic intrusive events have been dated at about 2.7 Ga (Rocci et al. 1991). At a regional scale, several episodes of isoclinal folding with NW-SE to N-S trending axes developed under high-grade metamorphic conditions. These tectonic events have been followed by the emplacement of several generations of basic dikes (1.6 Ga in age) and by uplift and intracratonic extension (Rocci et al. 1991).

Field Observations

During the expedition into the Reguibat-Adrar region, new observations about the regional geology were made. The

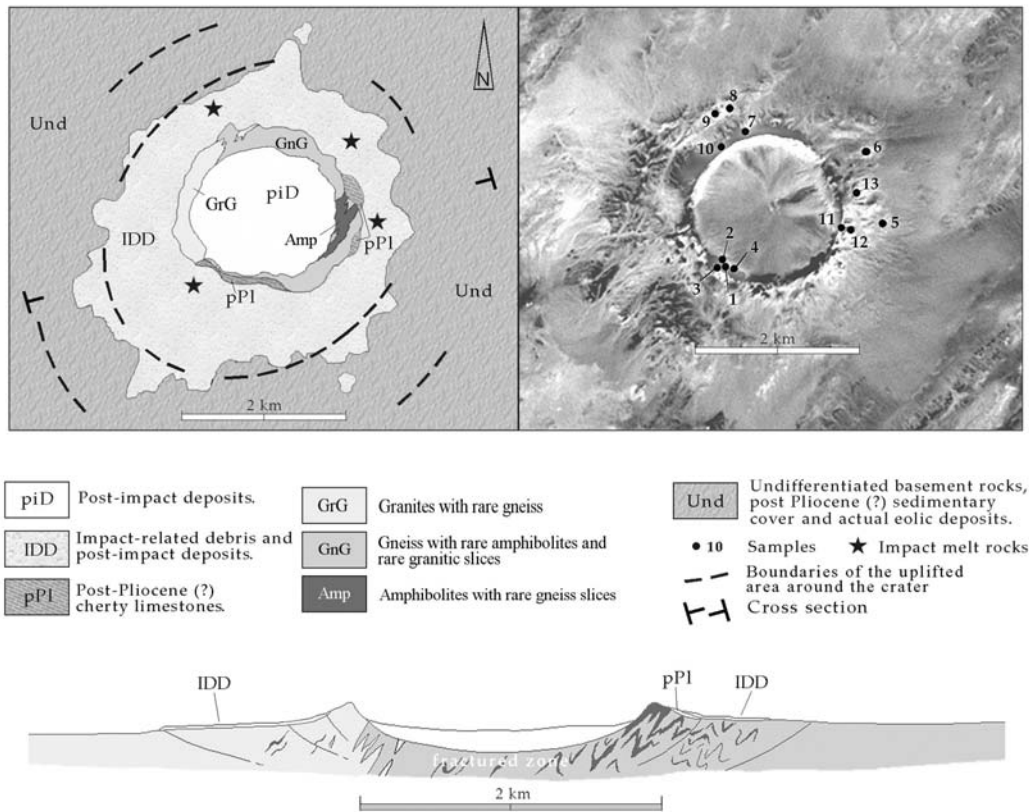


Fig. 4. Geological sketch map (left) and sketch with the sample locations on a satellite image (modified after NASA, <https://zulu.ssc.nasa.gov/mrsid/mrsid.pl>). The samples: 1-MSP 2310; 2-MSP 2311; 3-MSP 2312; 4-MSP 2313; 5-MSP 2314; 6-MSP 2315; 7-MSP 2316; 8-MSP 2317; 9-MSP 2318; 10-MSP 2319; 11-MSP 2320; 12-MSP 2321; 13-MSP 2322.

basement rocks consist mainly of granite, gneiss and mafic rocks that are massive or locally foliated. The metamorphic rocks are deformed into tight to isoclinal folds with NW-SE trending fold axes. The contact between gneissic and mafic rocks is generally sharp but was subject to deformation during the metamorphic events.

The metamorphic rocks locally are intruded by granitic dikes that are only slightly deformed by gentle to open folds and crosscut by late jointing associated to a relatively late faulting event of the Reguibat Shield. In the Tenoumer region, a 20–30 m thick succession, made up of alternating beds of limestones, cherty limestones, calcretes and silcretes, rests on the peneplain. Although Piqué (2001) suggested a Plio-Pleistocene age for the calcareous sedimentary cover of the Reguibat Shield, there are no specific age constraints for the sedimentary succession at Tenoumer. We only know that is older than the crater.

In the crater area, target rocks and impact melt breccias were recognized in outcrop. The target rocks can be observed along the inner and outer slopes of the crater rim, where good exposures of basement rocks, up to several hundred meters wide, are present. They are mainly granite, granitic gneiss, and mafic rocks. The latter ones crop out extensively in the northwest and eastern part of the outer rim (see Fig. 4). Joints

and shear fractures—showing a radial distribution and, therefore, probably related to the impact—occur pervasively along the entire rim with a preferred radial orientation. Along the southern portion of the rim, the layered, younger sedimentary, calcareous cover underlies a thick succession of debris, blocks and megablocks, of metamorphic basement rocks (granites, gneiss, amphibolites) ejected from the crater (Fig. 5).

Impact melt rock occurs in patches outside the crater, predominantly to the east, northwest, and southwest, lying on the basement rocks and on the sedimentary cover (Figs. 4 and 5), and cropping out all around the structure as boulders. All these lithologies are arranged chaotically among the hills formed by the ejecta. Lateral continuity of the rock bodies is limited to a few tens of meters. The rocks of these ejecta hills appear severely fractured (Figs. 6 and 8).

The sedimentary infill of the crater is mainly derived by rim erosion and wind transportation (Lancaster et al. 2002): eolian sands, rock debris and thin layers of evaporitic deposits are recognizable.

The well-preserved geomorphological features of the crater support the young age (21.4 ± 9.7 kyr) of the structure recently suggested by Storzer et al. (2003). In fact, because of the strong changes of the climate conditions during Pliocene-

Pleistocene times (Gasse 2000) and considering the relationship between climate evolution and geomorphological forms (e.g., precipitation rate versus erosion rate), the previous age of about 2.5 Ma, as suggested by French et al. (1970), seems too high.

Several samples of target and impact melt rocks were collected from different sites, mainly outside the crater (locations shown in Fig. 4). These specimens are now in the collection of the Museo di Scienze Planetarie, Prato (Italy) for research and exhibition. Impact melt samples were found predominantly on the eastern outer flank of the crater rim. To date, no ballistically dispersed melt samples with aerodynamic forms have been found.

SAMPLES AND ANALYTICAL TECHNIQUES

Twelve samples of target rock and six samples of impact melt rock were selected for this study. The samples were studied by optical microscopy and were analyzed for major and trace elements, including REE and PGE abundances.

Three samples of impact melt (two highly vesicular samples, MSP 2314 and MSP 2317, and one with low porosity, MSP 2315, belong to the collection of the Museo di Scienze Planetarie-Provincia di Prato (Italy); three others (NMNH 113029-18 with an extraordinary high porosity, NMNH 113029-15 with a medium amount of vesicles, and NMNH 113029-62 with a low amount of vesicles) are from the Department of Mineral Sciences (Division of Petrology and Volcanology) of the Smithsonian Institution, Washington, D.C. The samples collected by the authors are similar to those of the Smithsonian Institution, with the exception of specimen 113029-18, which appears to be particular due to its high porosity and composition and shows the lowest aluminum and alkali contents, as well as the highest calcium content of all the melt rocks analyzed (Table 3).

Sample Preparation

Forty thin sections of impact melt and country rock samples were prepared for optical and electron microscopy.

For major and trace element analysis, about 40–100 g of material (the samples provided by the Smithsonian Institution were only 40–50 g each) were crushed and then pulverized in an agate ball mill. In order to avoid contamination by the steel of the jaw crusher, the samples were embedded in multiple thick plastic bags and then crushed with a hammer. Contamination during the pulverization stage was avoided by cleaning the agate mill, between each sample, with high-purity silica powder and then rinsing it with deionized water.

The use of a relatively large amount of material appeared necessary, because the optical investigation showed strong heterogeneities; in particular, the presence of schlieren and poor mixing of glass and microcrystalline phases cause compositional variation on the micro- and meso-scales.

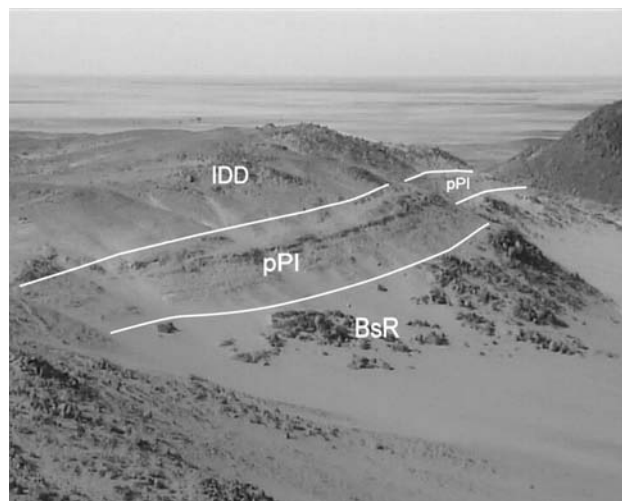


Fig. 5. The southern part of the rim. The impact-related debris (IDD) rests on the cherty limestones succession (pPI) and the latter on the basement rocks (BsR).

Moreover, as described by Tagle et al. (2003), PGE have the tendency to concentrate in small nuggets that can cause analytical problems.

Experimental Methods

Major elements were measured by lithium meta- and tetraborate fusion and ICP-AES at ALS Chemex Laboratory in Australia. Trace element abundances were determined after treating the rocks with HF-HNO₃-HClO₄ acid digestion and HCl leaching, and employing a combination of ICP-MS and ICP-AES at ALS Chemex in Australia; REE and Th, U, Y were measured by lithium metaborate fusion and ICP-MS at the same laboratory. Loss on ignition (LOI) was determined at a temperature of 1010 °C for one hour.

Platinum-group element analyses were done by ACTLABS in Canada (for more detail, see Koeberl et al. 1997; Koeberl and Reimold 2003) using a nickel sulfide fire assay collection procedure followed by inductively coupled plasma mass spectrometry analysis.

Accuracy of PGE analyses was verified through several analyses of the certified SARM-7 standard and amounts to ~10 rel%. Duplicate analyses of two melt rock samples were done to check analytical precision (less than 10 rel%). For the major element analyses, the following accuracy values were determined in (wt%): Si ±0.2; Ti ±0.05; Al ±0.4, Fe ±0.3, Mn ±0.05; Mg ±0.2; Ca ±0.03; Na ±0.04; K ±0.04.

PETROGRAPHIC OBSERVATIONS

The rocks from Tenoumer crater have in the past been described only by Monod and Pomerol (1966), French et al. (1970), and Fudali (1974). The last author, in particular, recognized an impact origin of the crater and suggested that



Fig. 6. On the left: a boulder of basement in which the relationships between the three different lithotypes cropping out at the Tenoumer are evident; in a “groundmass” of gneiss (GnG) are present lenses or slices of amphibolites (Amp) and of granites (GrG). On the right: boulder of gneiss showing portions with different textures.

mixing occurred between granitic-gneissic and amphibolitic components during the melt rocks formation. A summary description of our target and impact melt rocks is reported in Table 1.

Unshocked Basement Rocks

The target rocks from Tenoumer are represented by six main lithologies: 1) deformed granites; 2) orthogneiss, mostly derived from a granitic component; 3) mica schists, which are, from a structural point of view, transitional between orthogneiss and amphibolites; 4) amphibolites; 5) sedimentary components, including limestone and cherty limestone; 6) serpentinized ultrabasic rocks, outcropping only over a few tens of square meters. It is worth mentioning that granites and orthogneiss (granitoids) account for most of the target rock exposure, whereas amphibolites-ultrabasites and limestones represent minor components of the outcropping rocks. No impact-diagnostic shock deformation features were observed in our target rock samples.

Granites

At Tenoumer crater, a generally gradual and locally sharp (Fig. 6) transition between granites and gneiss, and between gneiss and mafic rocks is evident. A wide range of alternating lenticular bodies of granites (locally slightly foliated) and gneiss occurs; one notices an increase of well developed foliation and of micaceous minerals at the contacts between gneiss and amphibolites. It is worth noting that even where the contact between mafic and felsic rocks appears to be rather sharp, the mafic slices are embedded in decimeter to meter wide bands of mica schist.

The granites are pale gray to pinkish or brownish in color and are characterized by an inequigranular fabric with fine to

medium grain size. Larger crystals (up to 3–4 mm) are mostly quartz and plagioclase, with minor K feldspar and mica. A slight foliation locally affects the granites, which is most evident near contacts to gneiss. The contact zones are only up to 10 to 20 m wide and are marked by progressive changes of fabric and color.

Gneisses

The gneisses are the most widespread rocks occurring at the Tenoumer crater. They are pale gray to dark gray, rarely pinkish, showing a small-scale gneissic layering, with alternating felsic and mafic layers. The felsic layers have a granoblastic to lepidoblastic fabric and comprise millimeter-sized quartz, plagioclase, K feldspar, white mica and rare biotite. The mafic lepidoblastic sections are made up of biotite and muscovite, locally embedding feldspar porphyroblasts. The metamorphic and tectonic relationships between granites and gneiss suggest that the gneiss is derived from the progressive deformation of the granites.

More mafic portions, that are strongly deformed and stretched, form decimeter to hundreds of meter wide bodies. There are also abundant decimeter-sized “fish head” and “lenticular” (Ghosh 1993) boudins.

Mica Schists

The fabric of the gneiss changes abruptly in the vicinity of mica schists, and the granoblastic bands become very thin and rare. Locally, several meters wide mica schist is present at the transition to amphibolites. The mica schists crop out on the western and northern slopes of the rim of the crater and they are dark gray to dark greenish or brownish. A well developed foliation, defined by alternating bands of felsic (quartz and feldspar) and mafic (shiny dark to pale green micaceous minerals) minerals, is present. Very rare,

Table 1. Classification of samples from Tenoumer and summary of petrographic observations.

Catalogue no.	Field no.	Classification	Petrographic observations
MSP 2310	GP-1 (5-2A)	Granite	The hand specimen is pale grey to brownish and shows a fine to medium grained texture (larger crystals are up to 3–4 mm) composed of quartz, plagioclase, K feldspar and biotite, with minor muscovite. In thin section this sample has inequigranular subhedral crystals of quartz, plagioclase, K feldspar, biotite and muscovite. Locally Fe oxides and Fe hydroxides aggregate occurs. The felsic minerals are generally fractured and the plagioclase is locally altered. A later neo-blastesis of sub-euhedral micro-crystals of quartz and plagioclase is also present.
NMNH 113028-16		Granite Granodiorite ^a	Is a dark grey medium-grained granodiorite (plagioclase, K feldspar, quartz, and biotite), a rim rock immediately adjacent to and west of the southwestern rim pass.
MSP 2316	GP-7 (5-17)	Orthogneiss	The sample shows a fine to medium grained texture and a very slight gneissic layering, with alternating felsic minerals-rich layers and more mafic levels comprising biotite and muscovite with preferred orientation. The felsic layers are made of quartz, plagioclase microcline, rare K feldspar and biotite. At the microscope the sample has a prevalent granoblastic (only locally lepidoblastic) fabric. The granoblastic levels have equidimensional crystals of quartz, plagioclase (microcline) and K feldspar. Saussuritization of plagioclase often occurs. The lepidoblastic thin levels are made up of feldspar porphyroclasts, often weathered, biotite and muscovite. Epidote and zircon, as accessory phases, are also present.
MSP 2311	GP-2 (5-3)	Orthogneiss	The sample has a fine grained texture and a slight gneissic layering, with layers of felsic minerals separating layers rich in biotite. The felsic layers are made of quartz, plagioclase, K feldspar and rare biotite. At the microscope the sample shows a prevalent granoblastic (only locally lepidoblastic) fabric. The granoblastic levels have equidimensional crystals of quartz, plagioclase (microcline) and K feldspar. The lepidoblastic thin levels are made up of feldspar and biotite showing a preferred orientation and very rare and small crystal of subhedral pyroxene.
MSP 2319	GP-10 (5-19)	Orthogneiss	This brownish sample shows a fine grained texture and a gneissic layering, with alternating felsic and mafic layers. The felsic layers are comprised by quartz, plagioclase, K feldspar and rare biotite. The mafic levels are made of biotite and muscovite, locally embedding feldspar porphyroblasts. At the microscope the sample has a grano-lepidoblastic fabric. The granoblastic levels have equidimensional crystals of quartz, plagioclase (microcline) and K feldspar, with rare biotite/muscovite. The lepidoblastic thinner levels are made up of feldspar porphyroblasts and biotite/muscovite crystals embedding the felsic minerals. Locally chlorite also occurs. Finally, epidote crystals and Fe oxides aggregates occur.
MSP 2320	GP-16 (5-10)	Micaschist	This sample is made up of dark greenish to brownish micaschists, with a foliation defined by alternating levels of felsic (quartz and feldspar) and mafic minerals (shiny dark to pale green micaceous minerals), and very rare millimetric layers of phyllites. This sample represents the transitional term between orthogneiss and amphibolites. In thin section is evident a disjunctive cleavage defined by biotite/rare muscovite-rich layers and microlithons made up of quartz, acidic plagioclase, K feldspar and biotite. In the rare thinner phyllites levels a continuous cleavage defined by very fine-grained micaceous minerals is recognizable. Finally, micaschists comprise decimetric lens characterized by domainal spaced cleavage defined by biotite-rich layers and quartz/feldspar microlithons. Fe oxides and Ti minerals locally are present as aggregates.
MSP 2318	GP-9 (5-18)	Serpentinized ultrabasite	The hand specimen is light grey to light bluish, massive, apparently equigranular (with a very fine, up to aphanitic) fabric. Major minerals are those of the serpentine group. A fine network of thin fractures filled by dark minerals is present. In thin section this sample is characterized by a mylonitic texture with a fine matrix of antigorite, talc and minor chlorite. Porphyroclasts and relics of pyroxene and olivine partly or completely replaced by antigorite and talc are also present. A pervasive well-developed vein network is present and the veins are filled by antigorite and Fe oxides and hydroxides.

Table 1. *Continued.* Classification of samples from Tenoumer and summary of petrographic observations.

Catalogue no.	Field no.	Classification	Petrographic observations
MSP 2312	GP-3 (5-4)	Amphibolite with aplite vein	It is characterized by a whitish aplitic vein, with coarse anhedral crystals, intruded into a dark green to black granoblastic amphibolite with fine to medium (max. 2 mm) crystals. The aplite comprise quartz, plagioclase and rare K feldspar. In the amphibolite there are amphiboles with other microscopic crystals of mafic minerals. The contacts between aplite and country rocks are sharp. In thin section the major minerals of the aplite are quartz and plagioclase. Locally K feldspar and spots of Fe oxides and hydroxides are also present. In the amphibolite, the granoblastic fabric comprises amphiboles (tremolite/actinolite) along with little crystals of orthopyroxene and rare epidote.
NMNH 113028-2		Amphibolite ^a	Is an amphibolite forming a large vein in the granite gneiss rim crest just east of the northeastern rim pass.
MSP 2321	GP-17 (5-10B)	Amphibolite	The hand specimen is dark-greenish to black in color due to the dominance of dark green crystals of mafic minerals. It is characterized by a fine to medium inequigranular fabric with a local slight foliation. In thin section the major minerals are amphiboles (tremolite/actinolite), rare pyroxene and very rare quartz. Relics of altered crystals are present, generally embedded by mafic minerals with preferred orientation.
MSP 2322	GP-18 (5-15-A)	Amphibolite	The sample is greenish to black in color, due to the dominance of dark green crystals of mafic minerals with preferred orientation. A fine to medium inequigranular fabric with a local strong foliation is present. Veins filled by calcite crosscut the these rocks. The thin section show amphiboles (tremolite/actinolite), pyroxene relics (in the core partly substituted by tremolite/actinolite) and very rare quartz. Domainal spaced cleavage is defined by amphibole rich layers and porphyroclasts of quartz, amphibole and altered pyroxene are present and embedded by strongly oriented amphibole. The undeformed calcite veins cut the metamorphic fabric. Fe oxides and hydroxides are present in isolated spots.
MSP 2313	GP-4 (5-5)	Limestone	In hand specimen, this sample is characterized by a light gray to yellowish dominant lithotype made of prevalent calcareous breccia, and gray cherty nodules. The calcareous elements consist of clasts supported calcarenites and are cemented by microgranular calcite and locally dolomite. At the microscope the clast supported calcarenitic elements of the breccia, with a more or less marly matrix, consist of prevalent carbonatic equigranular elements with very rare silt-sized eolian clasts of rounded quartz and plagioclase. In the cement, consisting of microcrystals of calcite and dolomite, silty-sized eolian clasts of quartz and plagioclase are also present and Fe oxides aggregates occur.
MSP 2314	GP-5 (5-11)	Melt-matrix breccia	The hand specimen shows an highly vesicular texture.
MSP 2315	GP-6 (5-16)	Melt-matrix breccia	The specimen is quite compact and, as a consequence, its porosity is rather low.
MSP 2317	GP-8 (5-17B)	Melt-matrix breccia	Highly vesicular sample.
NMNH 113029-15		Impact melt ^a	The sample exhibits all the features of a shock melt. The principal constituent is a light brown feathery looking anomalously birefringent matrix, in which individual crystals cannot be distinguished. The specimen show a medium amount of vesicles.
NMNH 113029-18		Impact melt ^a	This sample looks like a scoria owing to the extremely high porosity, the highest of all the samples analyzed.
NMNH 113029-62		Impact melt ^a	Low amount of vesicles.

^aDescription of these rocks were taken from Fudali (1974).

millimeter wide layers of phyllites are also present near the contact with amphibolites.

Amphibolites

The amphibolites are generally very dark and greenish to black in color, but in a few outcrops they are light gray to light green. The dark color is due to the dominance of dark green, mafic, generally aligned minerals. These rocks are

characterized by a fine to medium grained, inequigranular fabric with a locally strong foliation defined by lepidoblastic bands of amphiboles, pyroxene, and other very little grains of felsic minerals (Fig. 6).

The entire basement to the crater structure, including all the above lithologies, is intruded by felsic dikes, mainly featuring micro-granites and aplites. They are, however, not very abundant.

Serpentinized Ultrabasites

On the northern, outer slope of the crater rim a peculiar rock crops out over only a few square meters. Its relationships with the surrounding rock are not evident, and this outcrop is the only one found. The rock is light gray to light bluish, massive, very fine grained, and displays an equigranular fabric. Major minerals are those of the serpentine group. It is characterized by a mylonitic texture with a fine matrix of chlorite and antigorite, in which porphyroclasts and relics of pyroxene and olivine are embedded. It is thought that this lithology could represent altered peridotite.

Limestones

On the eastern and southern slopes of the rim, a succession up to 30-m-thick of light gray to whitish, layered cherty limestone crops out. These rocks are surely older than the impact event: this is evident on the inner slopes of the rim, where the ejecta overlie the layered limestones and these are deformed by the impact (Fig. 5).

Impact Melt Rocks

Nature of the Matrix and Textures

The variety of impactites so far recognized in the Tenoumer area is quite restricted. According to the classifications of impactites proposed by Stöffler and Grieve (1994), the collected Tenoumer samples are all melt-matrix breccias (impact melt breccias or clast-rich impact melt rocks), containing both lithic and melt components (Fig. 7). These rocks do not contain discrete melt fragments in a clastic matrix, such as suevites (Stöffler et al. 1979; Stöffler and Grieve 1994).

These impact melt breccias are dark gray, both in outcrop and in hand specimen, and display a wide range of porosity, with voids varying from mm to cm in size. Thus, the appearance of the samples may be dense, slightly vesicular or, more rarely, so strongly vesicular that they resemble a pumice (Fig. 7). In all cases, the void density is probably related to the original amount of co-existing vapor phase inside the melts. The impact melt breccias occur typically as loose blocks, ranging from a few centimeters to several decimeters in size, on top of the basement rocks (Fig. 8). In particular, no large bodies or thick layers of melt have been observed, although their presence could be obscured by sand, mainly inside the crater. Based on the field relations, the Tenoumer impact melt breccias could represent a form of emplacement by injection into a conical or semiconical fracture system (Fudali 1974). The degree of crystallinity of the matrix of the impact melt rocks varies from almost completely crystalline to clear-brown glass containing only a few volume percent crystals, although large glass areas are very rare.

Thin section studies reveal that many clasts are granite or gneiss, although clasts of mafic precursor rocks (amphibolites) can be observed. The size of the inclusions

range from <1 mm up to several centimeters, and many of them show features distinctive of impact (PDFs in quartz; transformation of quartz to lechatelierite; “ballen”-structured quartz). Around the inclusions occur chilled areas, where a greater amount of glass is present. Moreover the glass, which can be clear or light brown, develops apophyses penetrating the fractures of the inclusions. Where the inclusions did not retain their original characteristics (such a conservation only occur in the inner portions of the larger fragments), selective mineralogical transformation may be developed.

According to the authors who previously studied Tenoumer crater (Monod and Pomerol 1966; French et al. 1970; Fudali 1974; French 1998), the typical melt rocks consist of a fine-grained intergrowth of plagioclase laths, pyroxene crystals, oxides, and glass (Fig. 7). The texture is intersertal to aphanitic and there are no features, like alignment of crystals, suggestive of flow structures.

Silicate-Carbonate Liquid Immiscibility

The sample NMNH 113029-15 from the southwestern outer rim of the crater reveals clear textural evidence for liquid immiscibility between the silicate-rich glass of the matrix and the carbonates. Calcite, in particular, forms spherules and globules within the silica-rich glass that sometimes can coalesce totally or partially (Fig. 9). Such textures, sometimes referred as ocellar or emulsion textures, have been observed in natural carbonatitic igneous rocks (Kjarsgaard and Hamilton 1989; Brooker 1998) as well as in impact melt rocks from Haughton (Osinski and Spray 2001) and Ries crater (Graup 1999). In the past, the presence of carbonates or sulfates in the impact melt glass has been considered as being the product of filling by secondary phases. In the case of Tenoumer crater, for example, Fudali (1974) described the melt rocks from the “southwestern dike swarm” of Tenoumer crater as characterized by some vesicles filled with secondary calcite and subordinate amounts of anhydrite.

CHEMISTRY OF TENOUMER SAMPLES

Major and Trace Elements

Results of the major and trace element analysis of target and impact melt rocks are reported in Tables 2 and 3. The six groups of target rocks show only little compositional variation within their groups but significant differences between the groups.

Major element abundances of impact melt rocks are in agreement with the range of values reported by Fudali (1974), who obtained a similar range of results (compare Table 3). Following Fudali (1974), the melt rocks associated with craters in Precambrian terrains exhibit almost invariably more mafic composition than the target country rocks, which are mainly felsic rocks. Analyses of major elements in impact

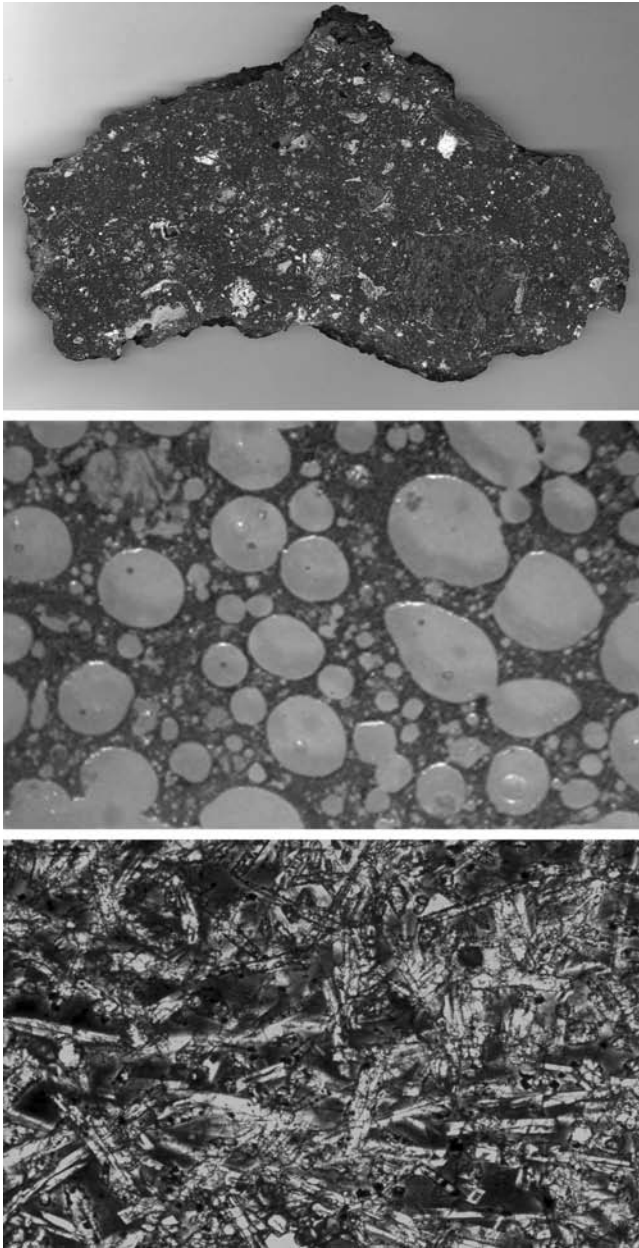


Fig. 7. From top to bottom: a slice (hand size) of an impact rock sample from Tenoumer; particular of the sample NMNH 113029-18, which exhibits the highest amount of voids among all the samples analyzed (width of view is 15 mm); sample NMNH 113029-62 consisting of elongated pyroxene and feldspar laths, opaque minerals and interstitial brown glass (width of view 400 μm).

melt rocks show lower contents of SiO_2 , Al_2O_3 and Na_2O , and higher contents of MgO , Fe_2O_3 , and CaO , than the felsic rocks (i.e., granites and gneisses) of the basement (Table 2); clearly the Mg, Fe, and Ca contents of the melt rocks are related to a contribution from mafic rocks and limestone (Figs. 10a and 10b; also see the section on mixing calculations). Other evidence of mixing is related to the titanium concentration of the impact melt rocks, which cannot be easily explained on the sole basis of the acid target



Fig. 8. The outcrops of the impact glasses are represented by isolated heaps of rocky fragments and debris.

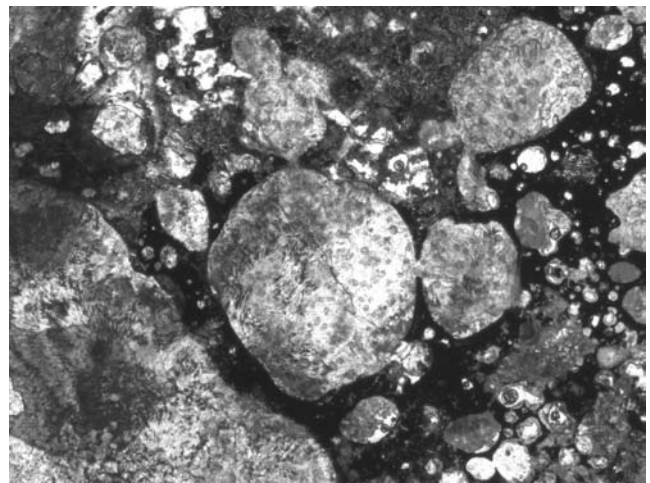


Fig. 9. Liquid immiscibility between silicate-rich glass and carbonates (sample NMNH 113029-15). Width of view is 2 mm.

formations, but it is reasonably due to incorporation of amphibolitic rocks that contain a high amount of TiO_2 ranging from 1.30 wt% for sample MSP 2321 to 2.69 wt% for sample MSP 2322 (Fig. 10c-Ti/Fe).

EDS analyses, performed by the authors on the glassy portions of the impact melt breccias, reveal that the silicate-rich glasses contain variable proportions of Si, Ti, Al, Fe, Ca, Na, and K. In comparison with the bulk analyses of the impact melt, the glass is strongly enriched in Si (SiO_2 ~70% in the glass versus ~60% of the bulk) and slightly enriched in Al (Al_2O_3 ~14% in the glass versus ~12% of the bulk), whereas it appears strongly depleted in Mg (MgO ~0.1% in the glass versus ~5% of the bulk) and depleted in Fe (FeO ~2% in the glass versus ~6% of the bulk) and Ca (CaO ~1% in the glass versus ~6% of the bulk).

The relatively high LOI of impact melt samples reflects the presence of calcite, mainly present as immiscible melt although the presence of calcite and gypsum as secondary

Table 2. Major and trace element composition of target rocks from the Tenoumer crater (oxides in wt%, trace elements in ppm).

	MSP 2310	MSP 2316	MSP 2311	MSP 2319	NMNH 113028-16	MSP 2320	MSP 2318	MSP 2312	NMNH 113028-2	MSP 2321	MSP 2322	MSP 2313
SiO ₂	69.05	70.65	70.76	69.22	69.11	51.96	51.18	56.12	47.55	49.51	47.10	47.31
TiO ₂	0.41	0.45	0.14	0.34	0.36	1.34	0.05	0.63	2.12	1.30	2.69	0.02
Al ₂ O ₃	15.62	14.17	16.11	15.17	15.05	16.80	1.35	10.27	9.86	8.24	9.35	0.35
Fe ₂ O ₃	3.60	3.07	1.46	3.27	3.77	9.76	7.71	10.73	14.62	13.05	13.02	0.52
MnO	0.04	0.04	0.01	0.04	0.03	0.12	0.11	0.27	0.18	0.18	0.23	0.04
MgO	0.79	0.63	0.52	1.13	1.05	3.60	32.16	8.17	11.72	14.87	10.80	1.02
CaO	2.84	1.61	2.62	3.51	2.91	5.99	0.12	9.71	7.43	7.28	8.94	27.93
Na ₂ O	4.83	2.47	4.84	4.52	4.41	3.83	0.02	2.13	2.81	2.31	3.15	0.05
K ₂ O	1.88	4.99	2.81	1.55	1.81	2.86	<0.01	1.05	0.28	0.13	0.13	0.07
P ₂ O ₅	0.16	0.13	0.07	0.10	0.17	1.02	<0.01	0.09	0.14	0.19	0.12	0.01
LOI	0.53	1.32	0.43	0.95	1.09	1.85	7.07	0.60	2.86	2.65	4.09	22.21
Total	99.75	99.53	99.77	99.80	99.76	99.13	99.77	99.77	99.57	99.71	99.62	99.53
Li	15.3	8.6	12.9	11.9	14.3	18.3	4.5	4.9	10.4	14.8	9.5	4.1
Be	1.55	1.55	1.19	0.94	1.17	1.86	0.10	1.14	1.13	1.16	0.92	0.43
S%	<0.01	<0.01	<0.01	<0.01	0.02	0.06	0.01	<0.01	0.05	0.04	0.03	0.08
V	49	36	22	48	45	187	27	202	258	165	288	20
Cr	3	3	4	15	12	2	1030	585	653	1050	675	18
Co	6.6	4.0	4.3	8.3	8.0	27.0	94.0	47.8	80.8	84.9	75.4	3.2
Ni	5.2	4.2	4.2	10.0	9.5	15.6	2100	176	633	817	611	4.5
Cu	22.5	34.1	5.9	13.7	17.5	31.6	9.1	8.5	275	331	522	4.0
Zn	56	42	22	43	52	112	74	127	110	89	78	19
Ga	23.8	20.1	19.2	18.1	20.2	23.7	3.32	17.2	16.8	13.4	15.9	0.62
Ge	0.40	0.46	0.33	0.12	0.25	0.59	0.15	0.52	0.44	0.43	0.39	0.09
As	0.6	<0.2	0.2	<0.2	1.2	1.1	0.5	<0.2	0.7	1.1	0.7	0.3
Se	<1	1	<1	<1	1	2	<1	1	2	1	2	<1
Rb	66.2	94.8	68.7	47.9	92.9	82.5	1.3	18.2	7.2	2.3	2.0	2.7
Sr	401	258	414	323	411	1390	6.9	191	484	235	354	244
Y	7.7	26.3	1.4	6.3	7.2	21.7	2.2	28.4	12.3	12.1	11.4	2.5
Zr	163	196	79.7	48.3	94.6	128	2.7	40.3	95.4	119	91.4	5.5
Nb	4.9	14.6	2.6	3.6	4.8	13.6	2.1	7.0	10.6	14.1	16.5	0.5
Mo	0.30	0.37	0.11	0.17	0.24	0.85	0.28	0.31	0.37	0.40	0.46	0.08
Ag	0.02	<0.02	<0.02	<0.02	0.07	0.18	<0.02	0.03	0.20	0.17	0.17	<0.02
Cd	0.02	0.03	0.03	0.03	0.06	0.10	0.03	0.22	0.09	0.09	0.05	0.09
In	0.02	0.02	<0.01	0.02	0.02	0.05	0.02	0.10	0.05	0.04	0.04	<0.01
Sn	1.3	1.9	0.6	0.8	1.0	1.8	0.8	3.3	1.4	1.2	0.8	0.3
Sb	<0.05	<0.05	<0.05	<0.05	<0.05	<0.05	<0.05	<0.05	0.07	0.07	<0.05	0.07
Te	<0.05	<0.05	<0.05	<0.05	0.07	0.09	<0.05	<0.05	0.12	0.07	0.08	<0.05
Cs	0.70	0.74	0.70	0.38	0.41	0.47	<0.05	0.14	0.08	0.13	0.27	0.09
Ba	678	2990	1310	750	1060	3940	266	335	984	75.8	749	2040
La	173	195	18.2	21.5	29.8	132	2.2	19.2	21.9	29.9	19.0	3.3
Ce	304	383	27.5	36.2	50.9	255	4.4	47.1	44.8	57.7	37.1	5.3

Table 2. *Continued.* Major and trace element composition of target rocks from the Tenoumer crater (oxides in wt%, trace elements in ppm).

	MSP 2310	MSP 2316	MSP 2311	MSP 2319	NMNH 113028-16	MSP 2320	MSP 2318	MSP 2312	NMNH 113028-2	MSP 2321	MSP 2322	MSP 2313
Pr	26.3	36.3	2.2	3.4	4.9	30.8	0.5	5.4	5.1	6.6	4.6	0.7
Nd	79.8	119	6.2	11.6	16.2	115	1.9	20.6	20.6	25.4	18.4	2.9
Sm	8.1	16.6	0.7	1.9	2.5	16.9	0.5	4.7	4.3	4.8	3.9	0.6
Eu	1.1	2.1	0.7	0.8	0.9	5.1	<0.1	1.2	1.5	1.3	1.2	0.3
Gd	6.4	12.9	0.6	1.9	2.2	12.3	0.5	4.9	3.8	4.3	3.6	0.5
Tb	0.5	1.4	0.1	0.3	0.3	1.3	<0.1	0.8	0.6	0.6	0.5	0.1
Dy	1.7	6.1	0.3	1.3	1.4	5.1	0.4	4.7	2.8	2.9	2.8	0.4
Ho	0.3	1.1	<0.1	0.2	0.3	0.9	<0.1	1.0	0.5	0.5	0.5	<0.1
Er	0.9	2.9	0.2	0.7	0.7	2.3	0.2	2.7	1.2	1.3	1.2	0.2
Tm	<0.1	0.4	<0.1	<0.1	<0.1	0.3	<0.1	0.4	0.2	0.2	0.2	<0.1
Yb	0.7	2.3	0.2	0.5	0.6	1.8	0.2	2.4	0.9	1.0	0.9	0.2
Lu	0.1	0.3	<0.1	<0.1	<0.1	0.3	<0.1	0.4	0.1	0.2	0.1	<0.1
Hf	4.7	5.6	2.6	1.2	2.9	3.4	<0.1	1.8	2.7	3.2	2.5	0.1
Ta	0.25	0.71	0.24	0.14	0.27	0.54	0.16	0.72	0.64	0.84	1.00	<0.05
W	0.2	0.8	0.1	0.1	<0.1	0.3	0.2	0.1	0.2	0.3	0.4	<0.1
Tl	0.34	0.42	0.36	0.23	0.30	0.43	<0.02	0.08	0.06	0.02	<0.02	0.02
Pb	23.1	24.3	17.1	9.9	10.5	19.4	1.3	9.3	5.5	3.1	2.1	1.7
Bi	0.02	0.03	0.01	0.03	<0.01	0.03	0.15	0.03	0.03	0.03	0.02	<0.01
Th	31.3	36.4	5.0	1.3	6.9	11.0	1.8	6.5	3.3	4.4	2.7	0.4
U	1.0	1.4	0.7	0.2	0.3	1.7	0.3	1.0	0.7	0.9	0.6	2.4
(La/Yb) _N	229.4	78.7	84.5	39.9	46.1	68.1	10.2	7.4	22.6	27.8	19.6	15.3
∑ REE	602.9	779.4	57.1	80.4	110.8	579.1	11.0	115.5	108.3	136.7	94.0	14.6
∑ LREE/ ∑ HREE	55.5	27.4	35.4	14.9	18.6	22.6	6.3	5.6	9.6	11.3	8.5	8.3

Table 3. Major and trace element composition of Tenoumer impact melts rock samples (major elements in wt%, trace elements in ppm).

	MSP 2314	MSP 2315	MSP 2317	NMNH 113029-15	NMNH 113029-18	NMNH 113029-62	FUD (range)
SiO ₂	58.02	62.17	58.24	60.92	60.44	61.78	58.02–64.76
TiO ₂	0.83	0.74	0.86	0.39	0.65	0.77	0.42–1.08
Al ₂ O ₃	12.51	12.60	12.42	13.41	11.08	12.51	11.36–13.96
Fe ₂ O ₃	7.39	6.83	7.67	3.89	6.70	7.26	3.89–9.17
MnO	0.09	0.09	0.10	0.04	0.08	0.09	0.04–0.12
MgO	5.68	5.17	5.94	1.85	5.04	5.26	1.96–6.95
CaO	6.89	5.47	6.50	7.80	7.91	5.27	4.03–7.29
Na ₂ O	3.39	3.35	3.53	3.59	2.85	3.39	3.14–3.94
K ₂ O	1.72	1.90	1.76	1.98	1.48	1.83	1.68–2.75
P ₂ O ₅	0.13	0.10	0.13	0.13	0.10	0.17	0.11–0.26
LOI	2.67	1.02	2.35	5.36	2.85	1.25	0.98–4.41
Total	99.32	99.44	99.50	99.36	99.18	99.58	
Li	10.9	5.8	10.0	15.6	8.2	6.6	
Be	1.13	1.09	1.04	1.08	1.15	1.26	
S%	0.14	0.11	0.07	0.08	0.22	0.06	
V	116	93	117	50	96	100	
Cr	327	291	331	41	257	291	
Co	36.9	32.6	37.1	10.7	32.6	33.0	
Ni	258	255	265	41.0	278	281	
Cu	86.7	57.7	88.5	14.9	64.6	52.0	
Zn	64	36	60	41	46	44	
Ga	18.7	15.8	17.6	16.6	15.3	16.3	
Ge	0.34	0.19	0.43	0.24	0.44	0.20	
As	0.5	<0.2	0.3	0.7	1.1	0.2	
Se	1	1	1	1	2	<1	
Rb	52.1	50.4	50.8	60.6	53.0	52.1	
Sr	450	393	392	425	471	445	
Y	14.4	13.9	13.6	11.9	12.4	13.0	
Zr	109	156	109	138	134	181	
Nb	10.4	9.3	9.9	6.5	8.4	9.9	
Mo	0.63	0.50	0.61	0.53	0.42	0.53	
Ag	0.03	<0.02	0.03	0.11	3.37	0.23	
Cd	0.04	0.03	0.02	0.06	0.10	0.07	
In	0.035	0.018	0.031	0.014	0.019	0.015	
Sn	0.5	1.0	1.3	1.0	2.9	1.0	
Sb	<0.05	<0.05	<0.05	<0.05	0.06	<0.05	
Te	<0.05	<0.05	<0.05	0.07	0.08	0.05	
Cs	0.65	0.48	0.62	0.33	0.46	0.43	
Ba	2110	1200	1590	3140	1880	1280	
La	42.5	44.9	43.4	53.4	37.2	44.4	
Ce	78.4	85.8	81.2	95.7	68.7	79.7	
Pr	7.7	8.6	8.1	9.4	7.0	8.6	
Nd	27.1	30.9	28.8	31.4	24.6	29.8	
Sm	4.6	5.0	5.0	4.8	4.4	4.8	
Eu	1.3	1.3	1.4	1.5	1.3	1.4	
Gd	4.2	4.5	4.4	4.1	3.8	4.4	
Tb	0.6	0.6	0.6	2.3	0.5	0.6	
Dy	2.7	2.8	2.7	2.4	2.5	2.7	
Ho	0.5	0.5	0.5	0.4	0.5	0.5	
Er	1.3	1.4	1.4	1.2	1.3	1.5	
Tm	0.2	0.2	0.2	0.2	0.2	0.2	
Yb	1.0	1.1	1.1	1.0	1.1	1.2	
Lu	0.2	0.2	0.2	0.2	0.2	0.2	
Hf	3.4	4.5	3.1	4.3	3.8	4.9	

Table 3. *Continued.* Major and trace element composition of Tenoumer impact melts rock samples (major elements in wt%, trace elements in ppm).

	MSP 2314	MSP 2315	MSP 2317	NMNH 113029-15	NMNH 113029-18	NMNH 113029-62	FUD (range)
Ta	0.57	0.52	0.53	0.34	0.46	0.53	
W	0.2	0.2	0.2	0.2	0.3	0.2	
Tl	0.17	0.12	0.14	0.18	0.11	0.15	
Pb	9.8	8.5	9.2	8.3	6.2	7.2	
Bi	<0.01	<0.01	<0.01	<0.01	0.02	<0.01	
Th	6.9	7.8	6.7	9.7	6.8	7.5	
U	0.9	1.0	0.8	0.8	1.1	0.9	
(La/Yb) _N	39.4	37.9	36.6	49.6	31.4	34.35	
∑ REE	172.3	187.8	179.0	208.0	153.3	180.0	
∑ LREE/∑ HREE	15.0	15.5	15.0	16.5	14.0	14.8	

minerals cannot be excluded. In fact, as previously reported, secondary calcite was suggested by Fudali (1974), whereas the occurrence of other secondary, hydrated minerals, such as gypsum, might be inferred from the sulfur abundances that are slightly higher in the impact melt samples than in the target rocks. Moreover, it is noticeable that the higher the amount of vesicles, the higher is the sulfur content. The importance of vesicles, which can represent a few volume percent of the rocks, as preferential sites for the formation of secondary minerals is further demonstrated by the lower LOI of the MSP 2315 and NMNH 113029-62 samples, which are the more massive samples.

Trace element concentrations in the samples show similar trends to those observed for major elements: in particular, little variation occurs within the six target rock groups. For example, the amphibolite group shows distinctly higher Co, Cr, Cu, Mn, Ni, and V contents, but lower Rb and Tl, compared to the gneiss and granite groups. The sedimentary component (i.e., limestone and cherty limestone) is well characterized by the major elements as well as by very low contents of Co, Cu, Ga, and Nb. The ultrabasite component is also distinct, apart from major element abundances, by having the highest contents of Co and Ni and the lowest contents of Be, Cs, Hf, P, Pb, Rb, Sr, and Zr in the entire sample suite. Therefore, the notable differences in the contents of each target rock group (felsic and mafic, respectively) can be used to constrain the contributions from these groups to the melt mixture (see section on mixing calculations).

As shown in Tables 2 and 3, some trace elements are enriched in the impact melt rocks with respect to the parent material, indicating complex mixing of these rocks during the melting process. Elements such as Co, Cu, Cr, Mn, Ni, and V are enriched in impact melt rock over felsic target rocks, but are depleted in comparison with the mafic rocks. Lead, Rb, and Tl contents of impact melt rocks are higher than the contents of these elements in the basic rocks but lower with respect to the contents of the acid rocks.

As previously emphasized by French et al. (1997), the high content of Ba is an interesting feature of the impactites.

Different from the other elements, the abundance of Ba is subject to strong variations also in the various rock groups. It can be derived from both the feldspar of the felsic rocks (see in particular the high content of orthogneiss sample MSP 2316 and mica schist sample MSP 2320) and from the sedimentary cover (MSP 2313) (Table 2).

Rare Earth Elements (REE)

The patterns of chondrite-normalized (Taylor and McLennan 1985) REE abundances of the Tenoumer target and impact melt rocks are shown in Figs. 11a and 11b, respectively. As indicated also by the La_N/Yb_N ratios of Tables 2 and 3, all samples exhibit higher normalized light REE (LREE) than heavy REE (HREE) abundances. Only gneisses and ultrabasite samples have negative Eu anomalies. Furthermore, due to the lithological variability of the target rocks, their REE patterns are quite varied (Fig. 11a). In contrast, the variation of REE patterns of impact melt rocks is significantly less (Fig. 11b) and attests their homogeneity. The overall REE abundances of gneiss and mica schist are much higher than those for the impact melt rock, and amphibolite shows an overall REE content similar to that of the impact melts, whereas the overall abundances for the other target rocks (granite, and mainly limestone and ultrabasite) are variably less than those for the impact melt rock samples.

The differences among the REE patterns of target and impact melt rock samples might appear in contrast to the results of other authors (Koljonen and Rosenberg 1976; Koeberl et al. 1985; Koeberl 1986; Val'ter and Kolesov 1990), who showed that the REE in vitreous impactites and tektites associated with meteorite craters usually have a concentration and composition strongly similar to the REE level and distribution of the target rocks. In particular, French et al. (1997) pointed out that the REE pattern of Gardnos impactites closely follows that of the granitic gneiss target rock. However, such an agreement is mainly due to the very high contribution (>80%) of the gneiss to the melt formation (French et al. 1997; Gilmour et al. 2003). In the samples from

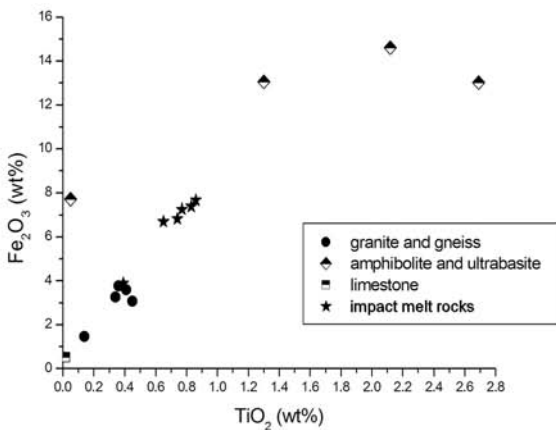
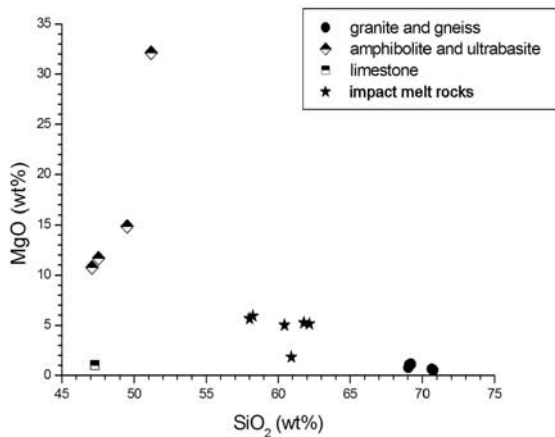
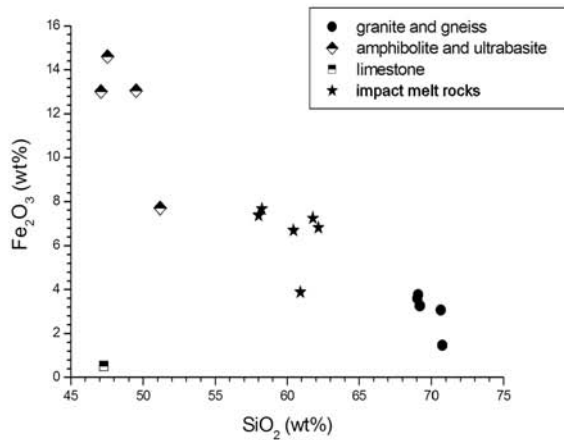


Fig. 10. a) SiO₂ versus Fe₂O₃; b) SiO₂ versus MgO; c) TiO₂ versus Fe₂O₃ data for target rocks and impact melt rocks.

Tenoumer crater, the discrepancy is only apparent, as the REE pattern of impact melt breccias represents complex mixing of the target rocks, as shown in the section on mixing calculations.

As reported in Table 4, the contents of PGE elements in the impact melt rocks from Tenoumer crater are unfortunately

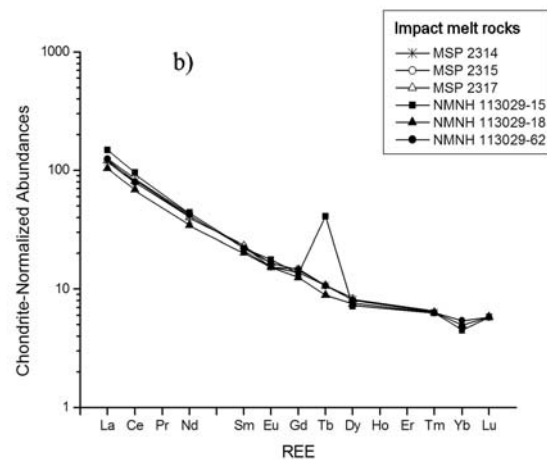
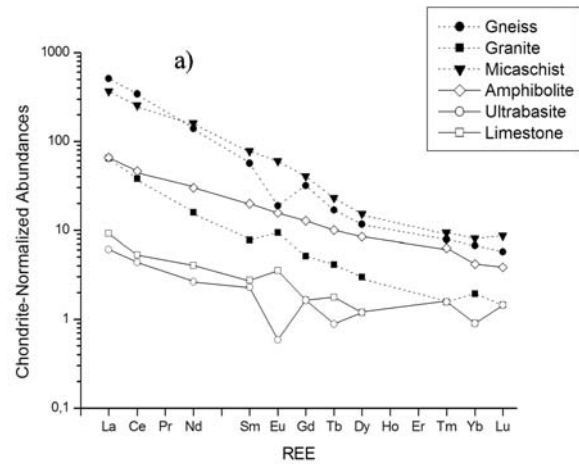


Fig. 11. Chondrite-normalized REE patterns of the target rocks (a) and impact melt rocks (b); normalization factors from Taylor and McLennan (1985).

very low. Re and Os data for our target and impact melt rocks are below the detection limits which are, respectively, 1 and 3 ppb, whereas the Ir content of the impact melt rocks is, at the maximum, in the range 0.1–0.2 ppb.

DISCUSSION

Mixing Calculations

Mixing models have sometimes been used in the study of impact melt and target rocks to establish contamination by the projectile or simply to evaluate the relationship with the parent rocks (e.g., Koeberl and Reimold 1995, 2003; French et al. 1997). The geological setting of the Tenoumer impact structure is in a complex geological terrain, involving Paleozoic metamorphic bedrock (gneiss dominated), metamorphic basic and ultra-basic material crosscut by granitic dykes, and a sedimentary component overlying the other country rocks. Therefore, in order to model the

Table 4. Platinum group elements and gold abundances in the samples from Tenoumer crater.

	MSP 2310	MSP 2316	MSP 2311	MSP 2319	MSP 2318	MSP 2312	MSP 2321	MSP 2313	Melt matrix breccia		
									MSP 2314	MSP 2315	MSP 2317
Au	<0.5	<0.5	<0.5	0.6	<0.5	<0.5	<0.5	2.0	0.9	1.7	<0.5
Ru	0.38	0.28	2.25	<0.05	0.21	2.18	3.12	0.24	0.46	1.16	6.39
Rh	<0.05	<0.05	<0.05	<0.05	0.69	0.52	0.47	0.12	0.14	0.37	0.03
Pd	<0.05	<0.05	<0.05	<0.05	0.37	2.83	2.94	0.79	0.54	0.23	<0.05
Re	<1	<1	<1	<1	<1	<1	<1	<1	<1	<1	<1
Os	<3	<3	<3	<3	<3	<3	<3	<3	<3	<3	<3
Ir	<0.05	<0.05	<0.05	<0.05	3.98	0.28	0.32	<0.05	0.12	0.17	<0.05
Pt	<0.05	<0.05	0.41	<0.05	0.70	7.42	7.64	0.61	1.04	1.10	0.16

All data in ppb.

composition of the impact melt rocks as a mixture of different proportions of target rocks, a series of mixing calculations has been performed using the average compositions of the following six possible target rock groups: 1) granite; 2) orthogneiss; 3) mica schist; 4) amphibolite; 5) limestone (limestone and cherty limestone); 6) serpentinized ultrabasic rocks.

Mixing calculations were performed with the HMX harmonic least-squares mixing calculation program by Stöckelmann and Reimold (1989). Useful information on the advantage of this program and suggestions on the refinement strategy have been given by, for example, French et al. (1997) or Koeberl and Reimold (2003). The elements that are more subject to post-impact overprint (typically mobile and volatile elements) are not useful for constraining target rock contributions and, therefore, these elements have been excluded in some runs. Due to their large variations between the different target rock groups, trace elements (such as La, Sm, Th, V, Co, Cr, Ni) have also been employed in some calculations for discrimination of individual component rocks. Finally, some runs (see Table 5) have been performed with separate gneiss and granite components.

Seven calculation runs were performed, and the results of these calculations, along with the number of components (target rock components) and mixture parameters (elemental abundances) employed for the different runs, are summarized in Table 5. Some calculations were performed with major element parameters only, others with major elements (except Na and K), and again others with major elements (with or without alkali) in combination with a number of trace elements (see footnotes to Table 5). Discrepancy factors, which represent a calculated measure for the validity of the results (the better and statistically more valid a result, the closer the corresponding discrepancy value approaches 0, as described by Stöckelmann and Reimold 1989) are quite good when compared to studies on other impact structures (Koeberl and Reimold 1995; French et al. 1997; Koeberl and Reimold 2003), although some results (Runs B, D, G) are not satisfactory. The absence of Na and K (Run C) did not produce an appreciable difference in comparison with other runs (A, E) where these elements were employed. The

addition of trace element data to the parameter list usually led to an increase in the discrepancy factor. However, some elements strongly worsen the mixing results: in Run F, the addition of La, Sm, Th, and V led to a discrepancy factor $FD = 1.5$, but when Co, Cr and Ni are added (Run G, see Tables 5 and 6), the discrepancy factor (mainly due to an enrichment of Cr and a depletion of Ni in observed values as compared with the calculated ones) increased up to 4.3, a very unsatisfactory result.

The results for the best runs (Runs A, C, E) are within the same range. Granitoids were found to be the most abundant component (about 50%), with additional mica schist (17–19%) and amphibolite (~15%). The sedimentary component (i.e., limestones, cherty limestones, calcretes, silcretes), which contributes with an amount of about 10%, and the ultrabasic (~6%) component are necessary to obtain a good mixing result. Due to their similar compositions, it does not make a significant difference whether the granitic and gneissic components are considered together (Runs A, B, C, D) or separately (Runs E, F, G). In Table 6, the calculated mixture compositions for three of the best calculation runs (Runs A, C, E) are compared with the observed melt rock composition. The discrepancies between the calculated and observed compositions are small for all elements, although a somewhat higher deviation for Fe_2O_3 is observed. Therefore, the mixture of the supracrustal and crustal lithologies present in the Tenoumer area does explain the melt rock composition.

Meteoritic Component

The detection of meteoritic components in impact-related rocks is very important, as it can help to confirm the impact origin for a certain structure and may give information about the type of impactor. So far, the presence of a meteoritic component has been established for just over 40 impact structures (Koeberl et al. 2001), although more than 170 have been currently identified on Earth. However, there may be several problems attached to the attempt to detect a meteoritic component. First of all, only minor amounts of the recondensed meteoritic vapor may be mixed with the target rocks. According to Attrep et al. (1991), the meteoritic

Table 5. Results of the HMX mixing calculations to reproduce Tenoumer impact melt breccia compositions.

	Target rock components							FD
	Granitoids	Granite	Gneiss	Amphibolite	Micaschist	Ultrabasite	Limestone	
Run A	51.34 ± 1.2	—	—	15.57 ± 0.5	17.59 ± 2.1	5.48 ± 0.3	10.03 ± 0.9	0.4
Run B	60.24 ± 0.8	—	—	28.84 ± 0.4	0.0	1.58 ± 0.3	9.35 ± 0.5	3.2
Run C	50.58 ± 1.4	—	—	14.66 ± 0.6	18.98 ± 2.5	5.71 ± 0.4	10.08 ± 1.1	0.4
Run D	59.50 ± 0.9	—	—	28.91 ± 0.4	0.0	1.55 ± 0.4	10.03 ± 0.6	3.0
Run E		11.16 ± 2.0	39.26 ± 1.6	14.64 ± 1.1	19.41 ± 1.7	5.73 ± 0.4	9.80 ± 0.3	0.4
Run F		10.30 ± 0.4	45.64 ± 0.7	21.12 ± 0.5	9.47 ± 0.6	4.13 ± 0.4	9.34 ± 0.5	1.5
Run G		12.00 ± 1.1	44.69 ± 0.9	25.61 ± 0.7	5.76 ± 0.8	2.86 ± 0.6	9.06 ± 0.7	4.3

From Run A to Run D: granitoids represent the average of the compositional data of the granitic and gneissic components. Run A: all major elements, included alkali elements; Run B: all major elements, included Na and K, plus Co, Cr, Ni, V; Run C: all major elements, except Na and K; Run D: all major elements (except Na and K) plus Co, Cr, Ni, V. From Run E to Run G: granite and gneiss composition have been considered separately. Run E: all major elements, included Na and K; Run F: all major elements (included Na and K) plus La, Sm, Th, V; Run G: all major elements (included Na and K) plus La, Sm, Th, Co, Cr, Ni, V. Limestone represents the sedimentary component with limestones, cherty limestones, calcretes and silcretes, as described in the text. FD = discrepancy factor (= goodness of fit; a lower number is best; see text). Harmonic least-squares mixing calculations (HMX) after Stöckelmann and Reimold (1989).

Table 6. Comparison of measured impact melt rock composition from the Tenoumer crater with those obtained from the mixing calculations.

	Run A		Run C		Run E		Run G	
	Calc.	$\Delta_{\text{obs-calc}}$	Calc.	$\Delta_{\text{obs-calc}}$	Calc.	$\Delta_{\text{obs-calc}}$	Calc.	$\Delta_{\text{obs-calc}}$
SiO ₂	60.00	0.25	59.91	0.35	59.92	0.34	60.52	-0.26
TiO ₂	0.72	-0.01	0.72	-0.01	0.72	-0.01	0.77	-0.06
Al ₂ O ₃	12.32	0.10	12.35	0.07	12.44	-0.02	12.09	0.33
Fe ₂ O ₃	5.96	0.65	5.97	0.65	5.86	0.75	5.97	0.65
MnO	0.08	0.001	0.08	0.001	0.08	0.001	0.08	-0.003
MgO	4.85	-0.03	4.85	-0.03	4.89	-0.07	4.89	-0.07
CaO	6.49	0.15	6.50	0.14	6.55	0.09	6.57	0.07
Na ₂ O	3.32	0.03			3.36	-0.01	3.42	-0.07
K ₂ O	1.79	-0.01			1.78	<0.001	1.56	0.22
La							46.14	-1.84
Sm							4.44	0.26
Th							7.64	-0.04
Co							28.89	1.61
Cr							241.57	14.43
Ni							240.50	-10.50
V							96.09	-1.09

Major elements in wt%; trace elements in ppm. The runs giving the best results, except for Run G (see text), were used for this comparison.

$\Delta_{\text{obs-calc}}$ = observed value minus calculated value.

component of the impactites can range widely; in particular, considering data for Meteor Crater, Wabar, Henbury, and Wolfe Creek, the meteoritic components range from about 0.06% to (exceptionally) 10%. Moreover, to reveal and differentiate such minute (or at least small) contributions from the compositional signature of the terrestrial target rocks can be very difficult.

Various siderophile trace elements, in particular the abundances of Co, Cr, and Ni, can be used to quantify the contribution from a projectile and to infer the nature of the projectile itself (e.g., Mittlefehldt et al. 1992; Koeberl and Fredriksson 1986; Palme et al. 1981; Meisel et al. 1990; Puura et al. 2004). Nevertheless, as concerns Co, Cr, and Ni abundances and ratios, extreme caution is required because sometimes their quantity can vary also within the crater—see for example the different contents in impact melt rock and

impact glass-rich breccias of Brent crater, as reported by Palme et al. (1981). Moreover, according to Attrep et al. (1991) and Mittlefehldt et al. (1992), complex vapor fractionation, depending on many factors (mass, nature, and velocity of projectile, temperature history, oxidation state of the target material) can occur. Sometimes, along with siderophile elements, even gold and selenium have been used by some authors (Tagle et al. 2003; Koeberl and Fredriksson 1986; Palme et al. 1981) to identify the presence of an extraterrestrial component in impact rocks. An enrichment of gold, the most volatile of the siderophile elements, in impact melts points to a possible meteoritic contamination; nevertheless this kind of contamination, if any, might be masked by a later depletion of this metal caused by weathering (Janssens et al. 1977; Palme et al. 1980).

The determination of platinum group element (PGE)

abundances and ratios is particularly useful for the identification of a meteoritic component. PGE are several orders of magnitude more abundant in meteorites than in terrestrial upper crustal rocks (Taylor and McLennan 1985; Koeberl 1998) and, therefore, their usage avoids some of the ambiguities that may result if only common siderophile elements (Cr, Co, Ni) are considered (Koeberl et al. 2001). A strong enrichment in siderophile elements in impact melt rock is usually indicative of a chondritic or an iron meteorite contamination (Palme 1982). In particular recent studies of PGE as well as Ni and Cr in impact melt revealed no fractionation between those elements (Tagle and Claeys 2002; McDonald et al. 2001), so their ratios in the melt might be representative of the composition of impacting asteroids. However, it is worth mentioning that contents of Cr, Co, and Ni in terrestrial rocks are generally variable and, moreover, the sources of these elements are uncertain (Koeberl 1998; Katongo et al. 2004). Therefore, in order to obtain unambiguous evidence for the incorporation of a meteoritic component, a support by PGE abundances is often necessary.

Although more abundant than in the felsic target rocks, the Pt content of impact melt rocks is not clearly indicative of an extraterrestrial component because the amphibolites have quite high abundances of this element: a contribution of about 15% amphibolite, as suggested by our mixing calculations (Table 5), can fully account for the Pt abundance in the melt breccias. As for Ir, the abundances in the impact melt rocks are compatible with a contribution by about 5% ultrabasic. The very low amount of Ir in the Tenoumer impact melt rocks is similar to those of many other craters. For example, Vredefort impact melt rock has Ir contents of 0.05 to 0.13 ppb (French et al. 1989), and Manicouagan impact melt rock has 0.02 to 0.03 ppb Ir (Palme 1982). An oddity is represented by the Au content of the Tenoumer impact melt rock samples: in two of them it is higher than in all other target rocks but the siliceous limestone. Anyway, considering its potential strong depletion in the melt due to fractionation (Mittlefehldt et al. 1992; Attrep et al. 1991) and the low contribution to the melt of the sedimentary component, which according to the mixing calculation results amounts to about 10%, it is anomalously high in the melt matrix breccias.

A further complication in revealing the possible contamination by meteoritic material is related to the weathering processes, which can affect the primary chemical composition: sample NMNH 113029-15, for example, shows some strong differences in major and minor element content with respect to the other impact melt rock samples. This sample, however, is affected by partial weathering, as also suggested by a relatively high LOI.

SUMMARY AND CONCLUSIONS

The present study has been focused on the geochemistry of the target rocks and melt matrix breccias from Tenoumer

impact crater, Mauritania. The target rocks of the highly metamorphosed crystalline basement chiefly comprise granite, gneiss, mica schist, amphibolite, and a rather rare ultrabasic component. All these rocks are overlain by a sedimentary component consisting chiefly of siliceous limestone and chert.

All of the samples have been investigated for up to 59 elements resulting in the most extensive data base of Tenoumer data published so far. The main target rock types can be well distinguished by their chemical compositions and, therefore, allowed detailed mixing calculations. The results showed that the melt-matrix breccia is derived from mixing of at least six different target lithologies outcropping in the area of the crater, with a large contribution to the melt from granitoids (50%), and significant mica schist (17–19%) and amphibolite (~15%) contributions, with minor contribution from cherty limestones (~10%) and ultrabasic (~6%).

A remarkable chemical feature of the impact melt rocks is represented by the REE patterns, which are symptomatic for the strong chemical homogeneity of this lithology, in comparison with the variable target rock compositions.

Low contents of PGEs in the impact melt rocks, in particular the very low Ir content, did not allow to confirm the presence of a meteoritic component, although the HMX-mixing calculations showed a noticeable enrichment of Cr and depletion of Ni in the impact melt indicating the occurrence of possible vapor fractionation.

As concerns the behavior of silicate and carbonate target rocks under shock conditions, the evidence of silicate-carbonate liquid immiscibility in the impact melt rocks, mainly as spherules and globules of calcite within the silicate glass, has been observed. Considering that mixing calculations showed a contribution from sedimentary cover around 10%, we inferred that such contribution is mainly present as immiscible sedimentary-derived melt.

Finally, an interesting feature of the Tenoumer geology relates to the amphibolites and ultrabasites which, in spite of their seemingly low proportion of the regional geology and their refractory character, in comparison to the felsic target rocks, have been involved in the formation of the impact melt. Two possible explanations can account for this observation: 1) the target is heterogeneous and the amphibolites were more abundant in the melt zone than they appear now; 2) in the particular conditions of an impact process, where high temperatures and pressures may be generated for very short periods of time, kinetics can play an important role thus leading to preferential fusion of mafic rocks, whose melts have a comparatively lower viscosity. Therefore, the possibility of a preferential contribution from mafic rocks during an impact process, where they occur together with felsic rocks, should be considered.

Acknowledgments—This paper is dedicated to Anna Maria Moretti, mother of G. Pratesi, who passed away in November 2002.

Thanks are due to the Department of Mineral Sciences (Division of Petrology and Volcanology) of the Smithsonian Institution for the loan of five samples from Tenoumer crater. We are also grateful, for the scientific support during the field expedition, to Luca Matassoni, Paolo Agnelli and Giuseppe Menotti Mazzini, and for logistic support to Riccardo Sabbadini, Karen Sameena Hassan and Luca Vagniluca.

The field expedition and the research work has been financed by the Museo di Scienze Planetarie of the Provincia di Prato, the Agenzia Spaziale Italiana, the University of Firenze, and the Italian Minister of University and Research.

Finally, we are strongly indebted to C. Koeberl, G. R. Osinski and W. U. Reimold for their critical and constructive comments. Thanks are also due to C. Koeberl and W. U. Reimold for providing us with the software for mixing calculations.

REFERENCES

- Allix A. 1951. Note et correspondance à propos des cratères météoritiques. *Revue Géographique de Lyon* 26:357–359.
- Attrep M., Jr., Orth C. J., Quintana L. R., Shoemaker C. S., Shoemaker E. M., and Taylor S. R. 1991. Chemical fractionation of siderophile elements in impactites from Australian meteorite craters (abstract). Proceedings, 22nd Lunar and Planetary Science Conference. pp. 39–40.
- Brooker R.A. 1998. The effect of CO₂ saturation on immiscibility between silicate and carbonate liquids: An experimental study. *Journal of Petrology* 39:1905–1915.
- Dietz R. S., Fudali R., Cassidy W. 1969. Richat and Semsiyat Domes (Mauritania): Not astroblemes. *Geological Society of America Bulletin* 80:1367–1372.
- French B. M. 1998. *Traces of catastrophe: A handbook of shock-metamorphic effects in terrestrial meteorite impact structures*. Houston, Texas: Lunar and Planetary Institute. 120 p.
- French B. M., Hartung J. B., Short N. M., and Dietz R. S. 1970. Tenoumer crater, Mauritania: Age and petrologic evidence for origin by meteorite impact. *Journal of Geophysical Research* 75: 4396–4406.
- French B. M., Orth C. J., and Quintana C. R. 1989. Iridium in the Vredefort bronzite granophyre: Impact melting and limits on a possible extraterrestrial component. Proceedings, 19th Lunar and Planetary Science Conference. pp. 733–744.
- French B. M., Koeberl C., Gilmour I., Shirey S. B., Dons J. A., and Naterstad J. 1997. The Gardnos impact structure, Norway: Petrology and geochemistry of target rocks and impactites. *Geochimica et Cosmochimica Acta* 61:873–904.
- Fudali R. F. 1974. Genesis of the melt rocks at Tenoumer crater, Mauritania. *Journal of Geophysical Research* 79:2115–2121.
- Fudali R. F. and Cassidy W. A. 1972. Gravity reconnaissance at three Mauritanian craters of explosive origin. *Meteoritics* 7:51–70.
- Fudali R. F. and Cressy P. J. 1976. Investigation of a new stony meteorite from Mauritania with some additional data on its find site—Ouelloul Crater. *Earth and Planetary Science Letters* 30: 262–268.
- Gasse F. 2000. Hydrogeological changes in the African tropics since the last glacial maximum. *Quaternary Science Reviews* 19:189–211.
- Gilmour I., French B. M., Franchi I. A., Abbott J. I., Hough R. M., Newton J., and Koeberl C. 2003. Geochemistry of carbonaceous impactites from the Gardnos impact structure, Norway. *Geochimica et Cosmochimica Acta* 67:3889–3903.
- Ghosh S. K. 1993. *Structural geology: Fundamentals and modern developments*. Oxford: Pergamon Press. 598 p.
- Graup G. 1999. Carbonate-silicate liquid immiscibility upon impact melting: Ries Crater, Germany. *Meteoritics & Planetary Science* 34:425–438.
- Grieve R. A. F., Garvin J. B., and Coderre Rupert J. M. J. 1989. Test of a geometric model for the modification stage of simple impact crater development. *Meteoritics* 24:83–88.
- Janssens M.-J., Hertogen J., Takahashi H., Anders E., and Lambert P. 1977. Rochechouart meteorite crater: Identification of projectile. *Journal of Geophysical Research* 82:750–758.
- Katongo C., Koeberl C., Witzke B. J., Hammond R. H., and Anderson R. R. 2004. Geochemistry and shock petrography of the Crow Creek Member, South Dakota, USA: Ejecta from the 74-Ma Manson impact structure. *Meteoritics & Planetary Science* 39: 31–51.
- Kennedy N. K. 1964. The structural differentiation of Africa in the Pan-African (6500 My) tectonic episode. 8th Annual Report on Research, Institute of African Geology, University of Leeds. pp. 48–49.
- Kjarsgaard B. A. and Hamilton D. L. 1989. The genesis of carbonatites by immiscibility. In *Carbonatites: Genesis and evolution*, edited by Bell K. London: Unwin Hyman. pp. 388–404.
- Koeberl C. 1986. Geochemistry of tektites and impact glasses. *Annual Reviews of Earth and Planetary Science* 14:323–350.
- Koeberl C. 1994. African meteorite impact craters: Characteristics and geological importance. *Journal of African Earth Sciences* 18: 263–295.
- Koeberl C. 1998. Identification of meteoritic components in impactites. In *Meteoritics: Flux with time and impact effects*, edited by Grady M. M., Hutchison R., McCall G. J. H., and Rothery D. A. GSA Special Publication #140. London: The Geological Society. pp. 133–153.
- Koeberl C., Fredriksson K. 1986. Impact glasses from Zhamanshin crater (USSR): Chemical composition and discussion of origin. *Earth and Planetary Science Letters* 78:80–88.
- Koeberl C. and Reimold W. U. 1995. The Newporte impact structure, North Dakota, USA. *Geochimica et Cosmochimica Acta* 59: 4747–4767.
- Koeberl C. and Reimold W. U. 2003. Geochemistry and petrography of impact breccias and target rocks from the 145 Ma Morokweng impact structure, South Africa. *Geochimica et Cosmochimica Acta* 67:1837–1862.
- Koeberl C., Kluger F., and Kiesel W. 1985. Rare earth elemental patterns in some impact glasses and tektites and potential parent materials. *Chemie der Erde* 44:107–121.
- Koeberl C., Armstrong R. A., and Reimold W. U. 1997. Morokweng, South Africa: A large impact structure of Jurassic-Cretaceous boundary age. *Geology* 25:731–734.
- Koeberl C., Reimold W. U., and Shirey S. B. 1998. The Ouelloul crater, Mauritania: On the problem of confirming the impact origin of a small crater. *Meteoritics & Planetary Science* 33:513–517.
- Koeberl C., Peucker-Ehrenbrink B., Reimold W. U., Shukolyukov A., and Lugmair G. W. 2001. Comparison of Os and Cr isotopic methods for the detection of meteoritic components in impact melt rocks from the Morokweng and Vredefort impact structures, South Africa (abstract #3048). Conference, Catastrophic Events and Mass Extinctions: Impacts and Beyond. LPI Contribution #1053. Houston, Texas: Lunar and Planetary Institute.
- Koljonen T. and Rosenberg R. I. 1976. Major elements and REE in tektites and three probable shock-metamorphic rock series of the Baltic shield. *Geochemical Journal* 10:1–11.
- Lancaster N., Locurek G., Singhui A., Pandey V., Deynoux M., Ghiene J. F., Lô K. 2002. Late Pleistocene and Holocene dune

- activity and wind regimes in the Western Sahara Desert of Mauritania. *Geology* 30:991–994.
- Master S. and Reimold W. U. 2000. The impact cratering record of Africa: an updated inventory of proven, probable, possible, and discredited impact structures on the African continent (abstract #3099). Conference, Catastrophic Events and Mass Extinctions: Impacts and Beyond. LPI Contribution #1053. Houston, Texas: Lunar and Planetary Institute.
- McDonald I., Andreoli M. A. G., Hart R. J., and Tredoux M. 2001. Platinum-group elements in the Morokweng impact structure, South Africa: Evidence for the impact of a large ordinary chondrite projectile at the Jurassic-Cretaceous boundary. *Geochimica et Cosmochimica Acta* 65:299–309.
- Meisel T., Koeberl C., and Ford R. J. 1990. Geochemistry of Darwin impact glass and target rocks. *Geochimica et Cosmochimica Acta* 54:1463–1474.
- Mittlefehldt D. W., See T. H., and Hörz F. 1992. Dissemination and fractionation of projectile materials in the impact melts from Wabar crater, Saudi Arabia. *Meteoritics* 27:361–370.
- Monod T., Pomerol C. 1966. Le cratère de Tenoumer (Mauritanie) et ses laves. *Société Géologique de France Série* 78:165–172.
- Osinski G. R. and Spray J. G. 2001. Impact-generated carbonate melts: Evidence from the Haughton structure, Canada. *Earth and Planetary Science Letters* 194:17–29.
- Paillou P., Malézieux J.-M., Reynard B., Dejaj J., El Barkooky A., Barakat A., and Heggy E. 2004. Discovery of the largest impact crater field on Earth in the Gilf Kebir region, Egypt. *Comptes Rendus Géosciences de l'Académie des Sciences* 336:1491–1500.
- Palme H. 1982. Identification of projectiles of large terrestrial impact craters and some implications for the interpretation of Ir-rich Cretaceous/Tertiary boundary layers. In *Geological implications of impacts of large asteroids and comets on the Earth*, edited by Silver L. T. and Schultz P. H. GSA Special Paper #190. Boulder, Colorado: Geological Society of America. pp. 223–233.
- Palme H., Rammensee W., and Reimold W. U. 1980. The meteoritic component of impact melts from European impact craters (abstract). Proceedings, 11th Lunar and Planetary Science Conference. pp. 848–850.
- Palme H., Grieve R. A. F., and Wolf R. 1981. Identification of the projectile at the Brent crater, and further considerations of projectile types at terrestrial craters. *Geochimica et Cosmochimica Acta* 45:2417–2424.
- Piqué A. 2001. *Geology of northwestern Africa*. Berlin-Stuttgart: Borntraeger. 310 p.
- Puura V., Huber H., Kirs J., Kärki A., Suuroja K., Kirsimäe K., Kivisilla J., Kleesment A., Konsa M., Preedon U., Suuroja S., and Koeberl C. 2004. Geology, petrography, shock petrography, and geochemistry of impactites and target rocks from the Kärda crater, Estonia. *Meteoritics & Planetary Science* 39:425–451.
- Richard-Molard J. 1948. Le cratère d'explosion de Tenoumer et l'existence probable d'une grande fracture rectiligne au Sahara occidental. *Comptes Rendues d'Académie des Sciences Paris* 227:213.
- Rocci G., Bronner G., and Deschamps M. 1991. Crystalline basement of the Western African Craton. In *The West African orogens and circum-Atlantic correlatives*, edited by Dallmeyer R. and Lécroché J. P. Berlin:Springer Verlag. pp. 32–61.
- Stöckelmann D. and Reimold W. U. 1989. The HMX mixing calculation program. *Journal of Mathematical Geology* 21:853–860.
- Stöffler D. and Grieve R. A. F. 1994. Classification and nomenclature of impact metamorphic rocks: A proposal to the IUGS subcommission on the systematics of metamorphic rocks (abstract). Proceedings, 25th Lunar and Planetary Science Conference. pp. 1347–1348.
- Stöffler D., Knöhl H. D., and Maerz U. 1979. Terrestrial and lunar impact breccias and the classification of lunar highland rocks. Proceedings, 10th Lunar and Planetary Science Conference. pp. 639–675.
- Storzer D., Sélo M., Latouche L., and Fabre J. 2003. The age of Tenoumer crater, Mauritania, revisited (abstract #1183). 34th Lunar and Planetary Science Conference. CD-ROM.
- Tagle R. and Claeys P. 2002. An L-chondrite origin for the Popigai crater (abstract). 2002 Annual Meeting of the Geological Society of America. pp.142–145.
- Tagle R., Stöffler D., Claeys P., and Erzinger J. 2003. A non-magmatic iron meteorite as impactor for the Rochechouart crater (abstract #1835). 34th Lunar and Planetary Science Conference. CD-ROM.
- Taylor S. R. and McLennan S. M. 1985. *The continental crust: Its composition and evolution*. Oxford: Blackwell. 312 p.
- Val'ter A. A. and Kolesov G. M. 1990. Distribution of rare earth elements in rocks from terrestrial astroblemes. *Geokhimiia* 7: 915–925. In Russian.
-